Nano Research 2015, 8(12): 3934–3943
DOI 10.1007/s12274-015-0894-8
Research Article
ISSN 1998-0124
CN 11-5974/O4

Integration of micro-supercapacitors with triboelectric nanogenerators for a flexible self-charging power unit

Jianjun Luo[1,§], Feng Ru Fan[1,2,§], Tao Jiang[1], Zhiwei Wang[1], Wei Tang[1], Cuiping Zhang[1], Mengmeng Liu[1], Guozhong Cao[1,3], and Zhong Lin Wang[1,4] (✉)

[1] *Beijing Institute of Nanoenergy and Nanosystems, Chinese Academy of Sciences, Beijing 100083, China*
[2] *Collaborative Innovation Center of Chemistry for Energy Materials, College of Chemistry and Chemical Engineering, Xiamen University, Xiamen 361005, China*
[3] *Department of Materials Science and Engineering, University of Washington, Seattle, Washington 98195, USA*
[4] *School of Material Science and Engineering, Georgia Institute of Technology, Atlanta, Georgia 30332, USA*
[§] *These authors contributed equally to this work.*

Received: 17 July 2015
Revised: 6 September 2015
Accepted: 8 September 2015

KEYWORDS
energy harvesting,
energy storage,
triboelectric nanogenerator (TENG),
micro-supercapacitor,
self-charging

ABSTRACT

The rapid development of portable and wearable electronic devices has increased demand for flexible and efficient energy harvesting and storage units. Conventionally, these are built and used separately as discrete components. Herein, we propose a simple and cost-effective laser engraving technique for fabricating a flexible self-charging micro-supercapacitor power unit (SCMPU), by integrating a triboelectric nanogenerator (TENG) and a micro-supercapacitor (MSC) array into a single device. The SCMPU can be charged directly by ambient mechanical motion. We demonstrate the ability of the SCMPU to continuously power light-emitting diodes and a commercial hygrothermograph. This investigation may promote the development of sustainable self-powered systems and provide a promising new research application for supercapacitors.

1 Introduction

In the last decade, flexible, portable, and wearable electronics have attracted increasing attention for use in various applications, such as electronic skin [1, 2], soft robotics [3], medical diagnosis [4, 5], and environmental monitoring [6, 7]. With the serious problems of environmental pollution and the possibility of an energy crisis, the desire for green and renewable energy sources for practical applications has gained increasing importance. The two most vital energy-sourcing technologies of harvesting and storage are usually addressed in two separated units based on two distinct processes.

The piezoelectric nanogenerator (PNG) [8, 9] was developed in 2006 to efficiently convert low-frequency

Address correspondence to zlwang@gatech.edu

mechanical energy into electricity as one potential solution to the problem of energy harvesting. The concept of self-charging power cells [10–13] followed, through which mechanical energy could be directly converted into electrochemical energy and stored. However, these devices have limitations: The PNG has insufficient power to charge the connected high-capacity storage unit. Recently, the novel energy-harvesting triboelectric nanogenerator (TENG) [14–16] was invented and widely utilized to efficiently collect mechanical energy. The working mechanism of the TENG relies on the coupling effect of contact electrification and electrostatic induction [17, 18]. In addition, the integration of a self-charging power unit [19] with a TENG device and a Li-ion battery was reported.

With the rapid development of miniaturized electronic devices, all-solid-state micro-supercapacitors (MSCs) have demonstrated great potential as complements to or replacements for batteries and electrolytic capacitors in many applications [20–22]. The devices possess remarkable advantages of high power densities, high rate capabilities, long cycle lives, and environmental friendliness.

From the perspective of materials, graphene offers tremendous potential for energy storage because it has high surface area and excellent electrical conductivity [23]. Recently, a simple and inexpensive production method for laser-induced graphene (LIG) was developed and implemented to fabricate high-performance supercapacitors [24, 25]. Unfortunately, conventional supercapacitors inevitably have limited lifetimes. In the context of portable electronics, a simple and cost-efficient fabrication method for a flexible self-charging micro-supercapacitor power unit (SCMPU) may be necessary for further developments in the field.

Considering these described problems, we have attempted to fabricate a flexible SCMPU using a laser engraving technique by integrating a TENG-based energy harvester and a MSC-array energy storage unit. A high degree of integration was realized through the double-faced laser engraving of a polyimide (PI) substrate. The two sides of the LIG electrodes were used separately for fabricating the TENG and MSC array. When ambient stress was applied to the SCMPU, the mechanical energy was directly converted into electrical energy and stored in the MSC array, which could be charged to 3 V in 117 min. Remarkably, the device demonstrated herein behaved with exceptional mechanical durability and electrochemical stability under several bending and pressing conditions. When fully charged, the SCMPU could continuously power two light-emitting diodes (LEDs) or a commercial hygrothermograph. The designed SCMPU showed great potential for powering wearable electronics, medical devices, and environmental or infrastructural sensors.

2 Experimental

2.1 Preparation of the polymer electrolyte

In a typical process, 5 mL H_2SO_4 (98 wt.%, Sigma Aldrich) and 5 g poly(vinyl alcohol) powder (M_W = 50,000, Sigma Aldrich) were added to 50 mL deionized (DI) water. Subsequently, the mixture was heated to 80 °C under continuous stirring until the solution became clear.

2.2 Fabrication of the MSC

LIG electrodes were directly written onto the surface of the Kapton PI (DuPont, 125 μm) substrates with a CO_2 laser cutter system (Universal PLS-6.75 laser system). The laser power was set to 5.0 W in all experiments. The PI substrates were first ultrasonically cleaned in acetone, ethanol, and DI water for 30 min each. In the MSC, LIG served as both the active electrode and current collector. For better electrical connection, silver paint was applied to the edges of the positive and negative electrodes. The electrodes were extended with copper tape. The interdigital area was defined with polyethylene terephthalate (PET) tape to protect the contact pad from the electrodes. Next, the polymer electrolyte was drop-cast on the active interdigitated electrode area, and left under ambient conditions for 12 h to ensure that the electrolyte completely wetted the electrodes and to evaporate the excess water. Finally, fluid polydimethylsiloxane (PDMS, Sylgard 184, Dow Corning) was spin-coated at 500 rpm onto the LIG-MSCs and cured at room temperature for 24 h.

2.3 Fabrication of the SCMPU

PI substrates were divided into the two groups PI 1 and PI 2 for different fabrication processes. For PI 1, LIG electrodes were produced on both sides. The upper surface was used for the MSC array. The MSC array was fabricated by the same process used above, but four written LIG patterns were connected in series. LIG was produced on the other side of PI 1 with an area of 3 cm × 3 cm as the top electrode. A layer of polytetrafluoroethylene (PTFE) film was pasted on the LIG. Finally, a water-based PTFE nanoparticle suspension was evenly sprayed onto the PTFE film, and dried by blown air. For PI 2, LIG was produced on a single side with an area of 3 cm × 3 cm as the bottom electrode. The PI 1 substrate was placed onto the PI 2, with the PTFE surface and LIG electrode facing each other. The device was sealed at both ends, forming an arched structure.

2.4 Characterization and measurement

Scanning electron microscopy (SEM) images were obtained using a HITACHI SU8020 and a FEI Quanta 450 FEG FE-SEM. High-resolution transmission electron microscopy (HRTEM) images were collected using a FEI Tecnai G2 F20 S-TWIN TMP FE-TEM. The open-circuit voltage (V_{OC}), short-circuit current (J_{SC}), and transferred charge density ($\Delta\sigma$) were measured by a Keithley 6514 electrometer. Cyclic voltammetry (CV) measurements were performed using an Autolab PGSTAT302N electrochemical workstation. Galvanostatic charge–discharge (CC) measurements were obtained using the LANHE CT2001A battery testing system.

3 Results and discussion

The device structure of the SCMPU is depicted in Fig. 1(a). The device contains two primary components of a flexible MSC array and an arched-structure TENG. These components were coupled through the double-faced laser engraving of the uppermost PI substrate by a commercial CO_2 laser cutter system. The two sides of LIG electrodes were used to fabricate the TENG and MSC array separately. A schematic of the laser engraving process is shown in Fig. S1 in the Electronic Supplementary Material (ESM). Figure 1(b) shows cross-sectional SEM images of the double-sided laser-engraved PI substrate. The thickness of LIG layers on both sides is ~40 μm and separated by an unexposed middle PI substrate that electrically isolates the two sides of the LIG. The higher-magnification SEM image inset in Fig. 1(b) displays the porous multilayered cross-sectional structure of the LIG. The SEM images in Fig. 1(c) depict the surface topography of the LIG, revealing a regular and porous microstructure written by the laser system, which benefits the performance of both the MSC array and the TENG. The HRTEM image in Fig. 1(d) reveals the few-layer features and ripple-like wrinkled structures of the thin LIG flakes. This characterization of the LIG is similar in morphology and graphene properties to that previously reported [24].

A photograph of a typical 3 cm × 3 cm SCMPU device is shown in the top inset of Fig. 1(a), demonstrating the flexibility and arch-shaped structure of the device. The dimensions of the SCMPU can be further reduced with the high resolution of the laser system used for production. To increase the triboelectric charge density in a large surface area and to enhance the mechanical robustness of the TENG, the surface of the PTFE thin

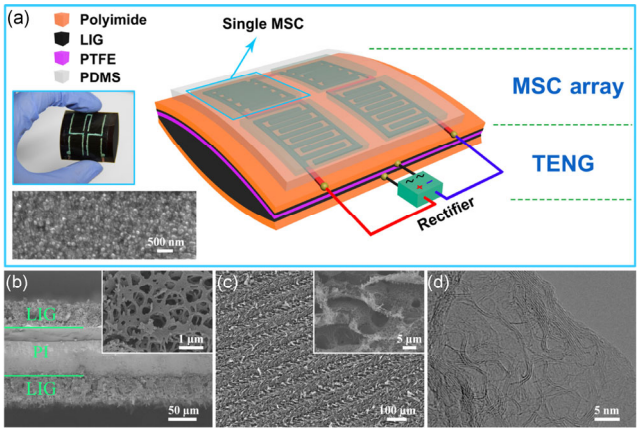

Figure 1 (a) Schematic depicting the detailed structure of the SCMPU. Top inset: photograph of SCMPU; bottom: SEM image of PTFE nanoparticles applied onto the surface of PTFE film. (b) Cross-sectional SEM image of a double-sided laser-engraved PI substrate with both sides of LIG. Inset: enlarged SEM image showing porous multilayer morphology of LIG. (c) SEM image of the LIG thin film. Inset: enlarged SEM image. (d) HRTEM image obtained from the edge of a LIG flake.

film was modified with a layer of PTFE nanoparticles [26], as illustrated in the bottom inset of Fig. 1(a). With this highly integrated SCMPU structure, the MSC array can be fully charged through the harvesting of ambient mechanical energy by converting the TENG-generated alternating current (AC) pulses to a direct current (DC) with a low-loss full-wave bridge rectifier. The working principle of the SCMPU is charted in Fig. S2 in the ESM.

To ensure the feasibility of the proposed device's structure, an energy-harvesting component with high-output performance is essential. Therefore, characterizing the outputs of the LIG-TENG is necessary. The electrical output measurement of the LIG-TENG was performed by a linear mechanical motor at 0.6 Hz.

In the process of contact–separation, a V_{OC} of ~168 V is generated between the two electrodes of the LIG-TENG (Fig. 2(a)). The $\Delta\sigma$ of ~68 $\mu C \cdot m^{-2}$ driven by this potential difference is also measured, as shown in Fig. 2(b). Consequently, the transfer of the charges produces an AC output with a peak J_{SC} of 21.3 $mA \cdot m^{-2}$ corresponding to the contact–separation process (Fig. 2(c)).

To further investigate the stability of the LIG-TENG, a periodical pressure was applied at 1 Hz. The voltage

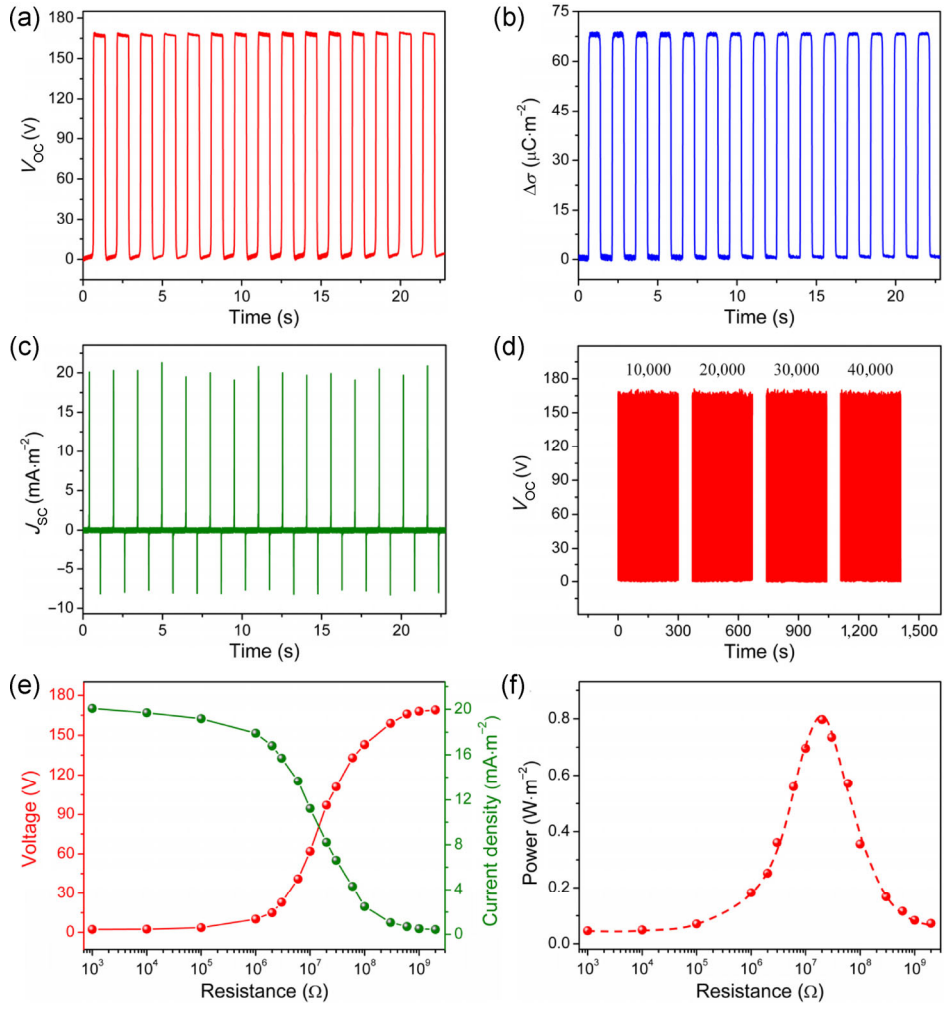

Figure 2 Output performance characterization of the LIG-TENG. (a) Open-circuit voltage (V_{OC}), (b) transferred charge density ($\Delta\sigma$), and (c) short-circuit current density (J_{SC}) generated by the LIG-TENG under periodical deformation at 0.6 Hz. (d) Mechanical durability characterization of the LIG-TENG. At a frequency of 1 Hz for 40,000 cycles, no degradation of the output voltage is experimentally observed. (e) The dependence of the output voltage and current density and (f) instantaneous power density of the LIG-TENG on the resistance of external load.

was recorded after each 10,000 loading/unloading cycles. In each recording, 300 cycles of data are presented, as shown in Fig. 2(d). The voltage amplitudes exhibit negligible change after 40,000 cycles, demonstrating the high repeatability, stability, and durability of the LIG-TENG unit.

Figure 2(e) illustrates the dependence of both voltage and current density outputs on a series of different resistances (from 10^3 Ω to 2 GΩ). The current density decreases drastically as the external resistance increases, while the voltage across the load experiences the opposite trend. Consequently, the effective electrical power density of the LIG-TENG relates closely to the external load, reaching a maximum value of 0.8 W·m^{-2} at a load resistance of 20 MΩ (Fig. 2(f)). Thus, the output performance of this LIG-TENG is comparable to that of the conventional metal-based TENG [27, 28] and much higher than that of the reported graphene-based TENG [29]. Most importantly, it is simple, cost-effective, and scale-controllable in production. This manufacturing technique may have promising prospects in the application of TENGs in other modes [30], such as the lateral-sliding and freestanding triboelectric-layer modes, because of the easy patterning of the LIG electrodes.

To further validate the feasibility of the device's structural design, we characterized the performance of the LIG-MSC. The architecture of the fabricated all-solid-state LIG-MSC is shown in Fig. 3(a). Figure 3(b) displays a photograph of the as-prepared LIG electrodes (single and four connected in series). A single LIG-MSC contains 10 interdigitated microelectrodes, including five each of positive and negative electrodes. The CV curves at different scan rates of 5, 10, 20, and 50 mV·s^{-1}, with quasi-rectangular shapes exhibiting the capacitive behavior of the device, are shown in Fig. 3(c), suggesting electrochemical double-layer (EDL) stability. Additionally, Fig. 3(d) shows the galvanostatic CC curves at current densities ranging from 0.02 to 0.20 mA·cm^{-2}. The CC curves present nearly ideal triangular shapes indicating excellent capacitive behavior. Inspection of the beginning of each discharge curve shows a negligible voltage drop, implying a very low internal resistance of the device.

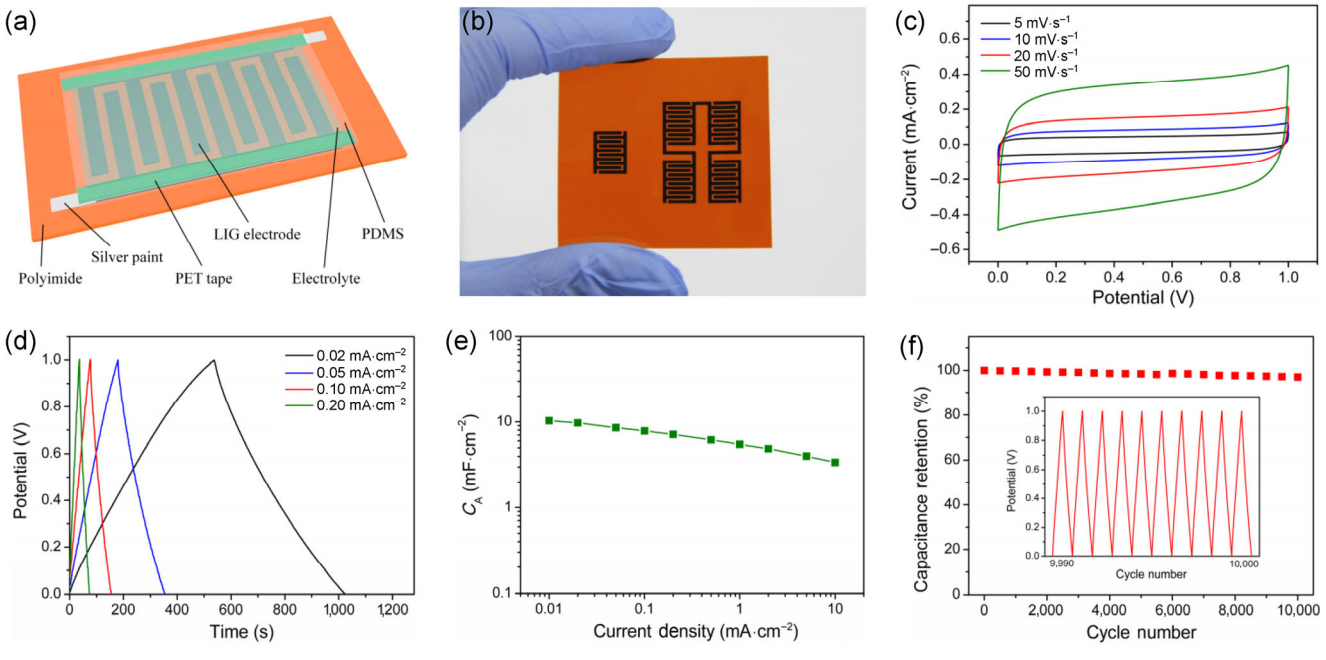

Figure 3 (a) Schematic and electrochemical performance of single all-solid-state LIG-MSC device. (b) Photograph of LIG interdigitated electrodes (single and four connected in series). (c) CV curves of LIG-MSCs at scan rates of 5, 10, 20, and 50 mV·s^{-1}. (d) Galvanostatic CC curves of LIG-MSCs at current densities of 0.02, 0.05, 0.10, and 0.20 mA·cm^{-2}. (e) Specific areal capacitances (C_A) calculated from CC curves as a function of the current density. (f) Cyclability testing of LIG-MSC with a CC current density of 0.05 mA·cm^{-2}, demonstrating only 3% loss of initial capacitance over 10,000 cycles. Inset: galvanostatic CC curves for the last 10 cycles.

The areal capacitances (C_A) of the LIG-MSC are calculated from the CC curves by the following equations

$$C = I\Delta t/\Delta V \quad (1)$$

$$C_A = C/S = I\Delta t/S\Delta V \quad (2)$$

where C is the total capacitance, I is the discharge current, Δt is the discharge time, ΔV is the potential window on discharging after IR drop, and S is the total area of the active positive and negative electrodes. The C_A is ~10.29 mF·cm^{-2} at a current density of 0.01 mA·cm^{-2} (Fig. 3(e)), comparable to or higher than those reported in the literature for carbon-based MSCs [21, 22, 24, 31, 32]. Furthermore, the single LIG-MSC shows excellent cyclic stability, retaining 97% of the initial capacitance after 10,000 charge/discharge cycles (Fig. 3(f)). A typical galvanostatic CC curve under continuous operation for the last 10 cycles is shown in the inset of Fig. 3(f). As seen from these results, the LIG-MSC displayed excellent performance suitable for integration with the self-charging system.

Considering that the SCMPU would sustain cyclic bending and pressing while working, we further demonstrated the durability of the LIG-MSC. Figure 4(a) depicts photographs of the LIG-MSC under the mechanical stresses of bending and pressing. The CV performance of the LIG-MSC indifferent bending and pressing conditions is shown in Fig. 4(b). The CV curves are similar to those obtained statically, indicating that bending and pressing have negligible effects on the capacitive behavior of the LIG-MSC. The performance durability is primarily attributed to the high mechanical flexibility of the all-solid-state LIG-MSC system and the elasticity of the protective PDMS layer. The C_A of the LIG-MSC was tested while maintaining a bent or pressed state. The capacitance retained 98% of the initial value after 6,000 cycles (Fig. 4(c)) under these conditions. These findings further demonstrate the potential of the LIG-MSC for energy storage in flexible, portable, and wearable electronics.

Practical applications often require energy storage units packaged in series, in parallel, or in combinations of the two to meet energy power requirements. Thus,

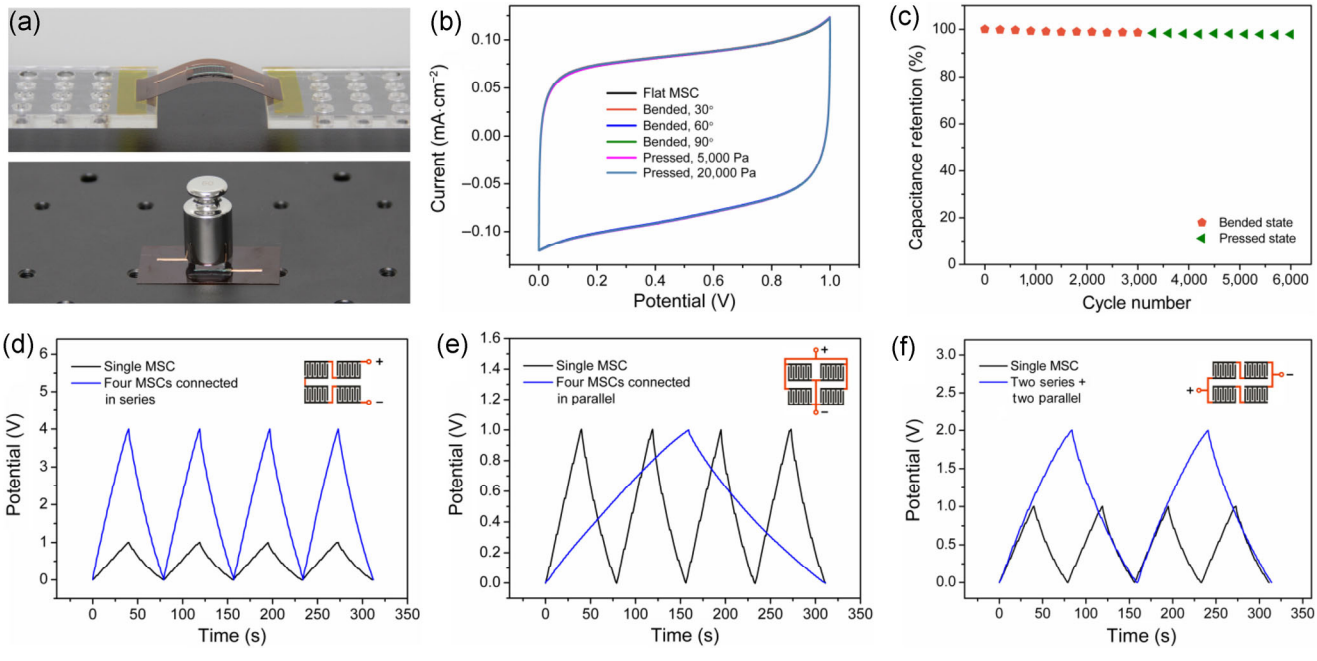

Figure 4 (a) Photographs of LIG-MSC bent to 30° and pressed with 5,000 Pa. (b) CV curves collected under different bending and pressing conditions at 10 mV·s^{-1}. (c) Performance durability of the MSC when tested under bending and pressing conditions (60° and 20,000 Pa) with a current density of 0.05 mA·cm^{-2}. (d)–(f) Galvanostatic CC curves of different MSC arrays (four single MSCs connected in series, in parallel, and combination of series and parallel, respectively) at current density of 0.10 mA·cm^{-2}. CC for single MSC is shown for comparison purposes.

MSC arrays of four single MSCs in series, parallel, or both were designed by the computer-controlled laser system. As shown in Figs. 4(d)–4(f), the operating potentials and currents are well controlled by the different configurations. The MSC arrays reveal nearly ideal triangular CC curves with minuscule voltage drops, indicating excellent capacitive properties and negligible internal resistances. The MSC arrays also exhibit excellent cycling stability (Fig. S3 in the ESM). With the resolution of the controllable laser system, the size of a single MSC can be further reduced and the MSC array can be easily adjusted into various combinations for specific applications (Movie S1 in the ESM).

To preferably match the performance of the MSC array, the output voltage of the LIG-TENG must be reduced. At present, two methods can be used to reduce TENG output voltage. The first method uses a transformer [33]. However, the use of a transformer not only causes substantial energy loss but also adds unnecessary weight and volume to the system. Furthermore, it is difficult to match the low-frequency and high-output load resistance properties of the TENG. The second method reduces the voltage by reducing the gap distance (d) of the TENG, which was proven successful in our previous works [34, 35]. This option is much more efficient for the self-charging system. To theoretically investigate the V_{OC}–d relationship of the LIG-TENG, a numerical calculation with finite element methods (FEM) was performed on the system. For simplicity, the LIG-TENG was treated as a parallel-plate capacitor in the established model, in which the PTFE plate with the LIG electrode was placed parallel to the counter LIG plate with varied d of 0 to 24 μm. The triboelectric charge density on the inner surface of PTFE plate was assigned as 68 μC·m^{-2}, equal to the measured transferred charge density from Fig. 2(b). The calculated potential distribution around the parallel-plate structure is displayed with color scaling in Figs. 5(a)–5(d). The potential difference between the top and bottom electrodes clearly decreases with decreasing d. By utilizing the numerical calculations, the experimental d of the LIG-TENG was reduced, with results shown in Figs. 5(e) and 5(f). When reducing d of the TENG component, the V_{OC} is reduced to ~30 V, which effectively matches that of the MSC array, while the J_{SC} was reduced to ~1.5 mA·m^{-2}. This AC output can be rectified to a unidirectional pulse output by a low-loss full-wave bridge rectifier (Fig. 5(g)) that generates electricity to be stored in the MSC array component. While working in the energy-harvesting mode (top inset of Fig. 5(h), S1 on; S2 off), the SCMPU converts the mechanical energy to electrical energy and stores it in the MSC array component. The charging curve of the MSC array component is shown in Fig. 5(h). The stored charge increases steadily with increased charging time, and the potential reaches 3 V in 117 min.

When a sufficient amount of charge has been stored in the energy storage mode, the SCMPU proceeds to the energy-supply mode (S1 off; S2 on). The circuit diagram of this mode is displayed in Fig. 6(a). Figure 6(b) demonstrates the fully charged SCMPU in use, simultaneously powering two LEDs with a minimum operating potential of 1.5 V. The painted area demonstrates the flexibility of the device. Even when bent to 90°, the device demonstrates ordinary behavior. The SCMPU can be inserted into the insole of a shoe (Fig. 6(c)), indicating potential applications for wearable electronics. To further demonstrate the application of the SCMPU, it was successfully utilized to continuously power a commercial hygrothermograph (Figs. 6(d)–6(f)), measuring the apparent difference in temperature and humidity between indoors and outdoors.

4 Conclusions

Using a simple and cost-effective laser engraving technique, we have developed a flexible SCMPU integrating a triboelectric-based energy-harvesting unit and an electrochemical storage unit into a single device. The SCMPU exhibited remarkable advantages such as self-charging capability, high durability, and environmental friendliness. The LIG-TENG had a peak power density of 0.8 W·m^{-2} at a loading resistance of 20 MΩ. The MSC had a high capacitance of ~10.29 mF·cm^{-2} at a current density of 0.01 mA·cm^{-2}. The TENG component efficiently generated electricity from ambient mechanical vibrations with high output; the rectified electrical energy was directly stored in the MSC array component, which could be charged

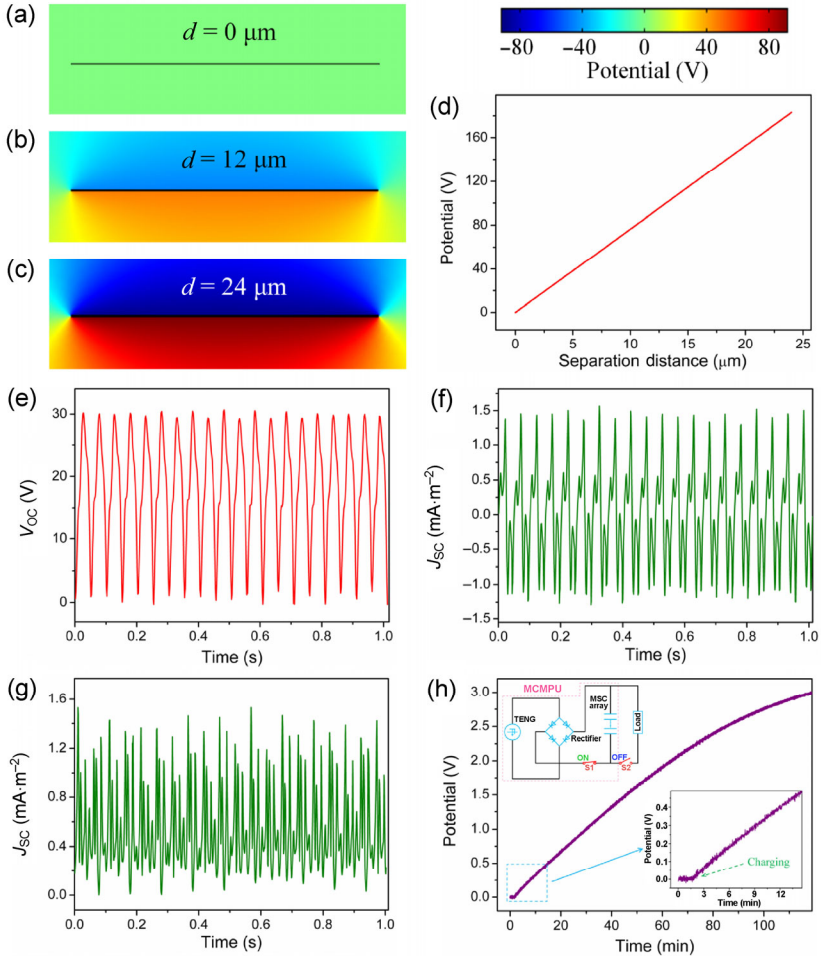

Figure 5 (a)–(d) Numerical calculations of the correlation between the potential difference and the gap distance d of the LIG-TENG. (e) V_{OC}, (f) J_{SC}, and (g) rectified J_{SC} generated by the TENG component when reducing d. (h) Charging curve of the MSC array component. Top inset: circuit diagram of the energy storage mode. Bottom inset: enlarged curve showing the potential rising.

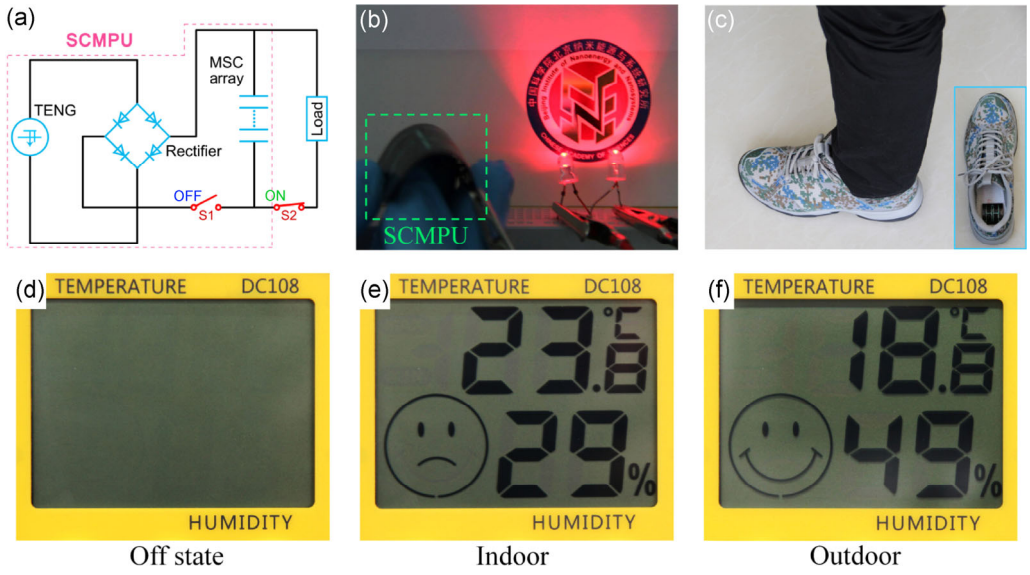

Figure 6 (a) Circuit diagram of the energy supply mode. (b) Photograph showing two LEDs being powered by the SCMPU. (c) Photograph of the SCMPU inserted in the insole of a shoe. (d)–(f) Photographs of using the SCMPU to drive a commercial hygrothermograph.

to 3 V in 117 min. When fully charged, the SCMPU could continuously power two LEDs and a commercial hygrothermograph. This work demonstrates a milestone in the development of mobile energy with profound potential influence on self-powered systems for flexible and wearable electronic devices.

Acknowledgements

This research was supported by the National Natural Science Foundation of China (Nos. 51432005 and 21403181), the "thousands talents" program for pioneer researcher and his innovation team, China, and Beijing Municiple Commission of Science and Technology project (Nos. Z131100006013004 and Z131100006013005). The authors would like to thank Chao Yuan, Weiming Du, and Yaguang Liu for helpful discussions and assistance in experiments.

Electronic Supplementary Material: Supplementary material is available in the online version of this article at http://dx.doi.org/10.1007/s12274-015-0894-8.

References

[1] Mannsfeld, S. C. B.; Tee, B. C. K.; Stoltenberg, R. M.; Chen, C. V. H. H.; Barman, S.; Muir, B. V. O.; Sokolov, A. N.; Reese, C.; Bao, Z. Highly sensitive flexible pressure sensors with microstructured rubber dielectric layers. *Nat. Mater.* **2010**, *9*, 859–864.

[2] Kang, D.; Pikhitsa, P. V.; Choi, Y. W.; Lee, C.; Shin, S. S.; Piao, L. F.; Park, B.; Suh, K.-Y.; Kim, T. I.; Choi, M. Ultrasensitive mechanical crack-based sensor inspired by the spider sensory system. *Nature* **2014**, *516*, 222–226.

[3] Ilievski, F.; Mazzeo, A. D.; Shepherd, R. E.; Chen, X.; Whitesides, G. M. Soft robotics for chemists. *Angew. Chem., Int. Ed.* **2011**, *50*, 1890–1895.

[4] Jeong, J. W.; Yeo, W. H.; Akhtar, A.; Norton, J. J. S.; Kwack, Y. J.; Li, S.; Jung, S. Y.; Su, Y. W.; Lee, W.; Xia, J. et al. Materials and optimized designs for human-machine interfaces via epidermal electronics. *Adv. Mater.* **2013**, *25*, 6839–6846.

[5] Chen, L. Y.; Tee, B. C. K.; Chortos, A. L.; Schwartz, G.; Tse, V.; Lipomi, D. J.; Wong, H. S. P.; McConnell, M. V.; Bao, Z. Continuous wireless pressure monitoring and mapping with ultra-small passive sensors for health monitoring and critical care. *Nat. Commun.* **2014**, *5*, 5028.

[6] Lee, M.; Bae, J.; Lee, J.; Lee, C. S.; Hong, S.; Wang, Z. L. Self-powered environmental sensor system driven by nanogenerators. *Energy Environ. Sci.* **2011**, *4*, 3359–3363.

[7] Pang, C.; Lee, G. Y.; Kim, T. I.; Kim, S. M.; Kim, H. N.; Ahn, S. H.; Suh, K. Y. A flexible and highly sensitive strain-gauge sensor using reversible interlocking of nanofibres. *Nat. Mater.* **2012**, *11*, 795–801.

[8] Wang, Z. L.; Song, J. H. Piezoelectric nanogenerators based on zinc oxide nanowire arrays. *Science* **2006**, *312*, 242–246.

[9] Wang, X. D.; Song, J. H.; Liu, J.; Wang, Z. L. Direct-current nanogenerator driven by ultrasonic waves. *Science* **2007**, *316*, 102–105.

[10] Xue, X. Y.; Wang, S. H.; Guo, W. X.; Zhang, Y.; Wang, Z. L. Hybridizing energy conversion and storage in a mechanical-to-electrochemical process for self-charging power cell. *Nano Lett.* **2012**, *12*, 5048–5054.

[11] Xue, X. Y.; Deng, P.; He, B.; Nie, Y. X.; Xing, L. L.; Zhang, Y.; Wang, Z. L. Flexible self-charging power cell for one-step energy conversion and storage. *Adv. Energy Mater.* **2014**, *4*, 1301329.

[12] Xing, L. L.; Nie, Y. X.; Xue, X. Y.; Zhang, Y. PVDF mesoporous nanostructures as the piezo-separator for a self-charging power cell. *Nano Energy* **2014**, *10*, 44–52.

[13] Ramadoss, A.; Saravanakumar, B.; Lee, S. W.; Kim, Y. S.; Kim, S. J.; Wang, Z. L. Piezoelectric-driven self-charging supercapacitor power cell. *ACS Nano* **2015**, *9*, 4337–4345.

[14] Fan, F. R.; Tian, Z. Q.; Wang, Z. L. Flexible triboelectric generator. *Nano Energy* **2012**, *1*, 328–334.

[15] Wang, Z. L. Triboelectric nanogenerators as new energy technology for self-powered systems and as active mechanical and chemical sensors. *ACS Nano* **2013**, *7*, 9533–9557.

[16] Fan, F. R.; Luo, J. J.; Tang, W.; Li, C. Y.; Zhang, C. P.; Tian, Z. Q.; Wang, Z. L. Highly transparent and flexible triboelectric nanogenerators: Performance improvements and fundamental mechanisms. *J. Mater. Chem. A* **2014**, *2*, 13219–13225.

[17] Grzybowski, B. A.; Winkleman, A.; Wiles, J. A.; Brumer, Y.; Whitesides, G. M. Electrostatic self-assembly of macroscopic crystals using contact electrification. *Nat. Mater.* **2003**, *2*, 241–245.

[18] Zhu, G.; Pan, C. F.; Guo, W. X.; Chen, C. Y.; Zhou, Y. S.; Yu, R. M.; Wang, Z. L. Triboelectric-generator-driven pulse electrodeposition for micropatterning. *Nano Lett.* **2012**, *12*, 4960–4965.

[19] Wang, S. H.; Lin, Z. H.; Niu, S. M.; Lin, L.; Xie, Y. N.; Pradel, K. C.; Wang, Z. L. Motion charged battery as sustainable flexible-power-unit. *ACS Nano* **2013**, *7*, 11263–11271.

[20] Chmiola, J.; Largeot, C.; Taberna, P. L.; Simon, P.; Gogotsi, Y. Monolithic carbide-derived carbon films for micro-supercapacitors. *Science* **2010**, *328*, 480–483.

[21] Gao, W.; Singh, N.; Song, L.; Liu, Z.; Reddy, A. L. M.; Ci, L. J.; Vajtai, R.; Zhang, Q.; Wei, B. Q.; Ajayan, P. M. Direct laser writing of micro-supercapacitors on hydrated graphite oxide films. *Nat. Nanotechnol.* **2011**, *6*, 496–500.

[22] El-Kady, M. F.; Kaner, R. B. Scalable fabrication of high-power graphene micro-supercapacitors for flexible and on-chip energy storage. *Nat. Commun.* **2013**, *4*, 1475.

[23] Zhu, Y. W.; Murali, S.; Stoller, M. D.; Ganesh, K. J.; Cai, W. W.; Ferreira, P. J.; Pirkle, A.; Wallace, R. M.; Cychosz, K. A.; Thommes, M. et al. Carbon-based supercapacitors produced by activation of graphene. *Science* **2011**, *332*, 1537–1541.

[24] Lin, J.; Peng, Z. W.; Liu, Y. Y.; Ruiz-Zepeda, F.; Ye, R. Q.; Samuel, E. L. G.; Yacaman, M. J.; Yakobson, B. I.; Tour, J. M. Laser-induced porous graphene films from commercial polymers. *Nat. Commun.* **2014**, *5*, 5714.

[25] Peng, Z. W.; Lin, J.; Ye, R. Q.; Samuel, E. L. G.; Tour, J. M. Flexible and stackable laser-induced graphene supercapacitors. *ACS Appl. Mater. Interfaces* **2015**, *7*, 3414–3419.

[26] Zhu, G.; Zhou, Y. S.; Bai, P.; Meng, X. S.; Jing, Q. S.; Chen, J.; Wang, Z. L. A shape-adaptive thin-film-based approach for 50% high-efficiency energy generation through micro-grating sliding electrification. *Adv. Mater.* **2014**, *26*, 3788–3796.

[27] Wang, S. H.; Lin, L.; Wang, Z. L. Nanoscale triboelectric-effect-enabled energy conversion for sustainably powering portable electronics. *Nano Lett.* **2012**, *12*, 6339–6346.

[28] Zhang, C.; Zhou, T.; Tang, W.; Han, C. B.; Zhang, L. M.; Wang, Z. L. Rotating-disk-based direct-current triboelectric nanogenerator. *Adv. Energy Mater.* **2014**, *4*, 1301798.

[29] Kim, S.; Gupta, M. K.; Lee, K. Y.; Sohn, A.; Kim, T. Y.; Shin, K. S.; Kim, D.; Kim, S. K.; Lee, K. H.; Shin, H. J. et al. Transparent flexible graphene triboelectric nanogenerators. *Adv. Mater.* **2014**, *26*, 3918–3925.

[30] Wang, S. H.; Lin, L.; Wang, Z. L. Triboelectric nanogenerators as self-powered active sensors. *Nano Energy* **2015**, *11*, 436–462.

[31] Pech, D.; Brunet, M.; Durou, H.; Huang, P.; Mochalin, V.; Gogotsi, Y.; Taberna, P. L.; Simon, P. Ultrahigh-power micrometre-sized supercapacitors based on onion-like carbon. *Nat. Nanotechnol.* **2010**, *5*, 651–654.

[32] Wu, Z. S.; Parvez, K.; Feng, X. L.; Müllen, K. Graphene-based in-plane micro-supercapacitors with high power and energy densities. *Nat. Commun.* **2013**, *4*, 2487.

[33] Zhu, G.; Chen, J.; Zhang, T. J.; Jing, Q. S.; Wang, Z. L. Radial-arrayed rotary electrification for high performance triboelectric generator. *Nat. Commun.* **2014**, *5*, 3426.

[34] Lin, L.; Xie, Y. N.; Wang, S. H.; Wu, W. Z.; Niu, S. M.; Wen, X. N.; Wang, Z. L. Triboelectric active sensor array for self-powered static and dynamic pressure detection and tactile imaging. *ACS Nano* **2013**, *7*, 8266–8274.

[35] Luo, J. J.; Fan, F. R.; Zhou, T.; Tang, W.; Xue, F.; Wang, Z. L. Ultrasensitive self-powered pressure sensing system. *Extreme Mech. Lett.* **2015**, *2*, 28–36.